

Characterization of a photon pair source based on a cold atomic ensemble using a cascade level scheme

Alessandro Cerè,¹ Bharath Srivathsan,^{1,2} Gurpreet Kaur Gulati,^{1,3} Brenda Chng,¹ and Christian Kurtsiefer^{1,4}

¹Centre for Quantum Technologies, National University of Singapore, 3 Science Drive 2, Singapore 117543

²current address: Max Planck Institute for the Science of Light, 91058 Erlangen, Germany

³current address: Jet Propulsion Laboratory, Caltech, Pasadena, California 91109, USA

⁴Department of Physics, National University of Singapore, 2 Science Drive 3, Singapore 117551*

(Dated: June 7, 2018)

We characterize a source of photon pairs based on cascade decay in a cold ^{87}Rb ensemble. This source is particularly suited to generate photons for interaction with ^{87}Rb based atomic systems. We experimentally investigate the dependence of pair generation rate, single photon heralding efficiency, and bandwidth as a function of the number of atoms, detuning and intensity of the pump beams. The observed power and detuning behaviors can be explained by the steady state solution of an established three-level model of an atom. Measurements presented here provide a useful insight on the optimization of this kind of photon pair sources.

I. INTRODUCTION

Time-correlated and entangled photon pairs are an important resource for a wide range of quantum optics experiments, ranging from fundamental tests [1, 2] to applications in quantum information [3–5]. A common method to obtain photon pairs is Spontaneous Parametric Down Conversion (SPDC) in nonlinear optical crystals [6], which have proven to be extremely useful. However, photons prepared by SPDC typically have spectral bandwidths ranging from 0.1 THz to 2 THz [7, 8], making interaction with atomic systems with a lifetime-limited bandwidth on the order of few MHz difficult. Possible solutions to match the bandwidth requirements include the use of optical cavities around the crystal [9–11], filters [12, 13], and recently the use of miniature monolithic resonators made of nonlinear optical materials [14]. A different approach uses directly atomic systems as the non-linear optical medium in the parametric process. There, a chain of near-resonant optical transitions provides an optical nonlinearity that has long been used for frequency mixing in otherwise inaccessible spectral domains. When two of the participating modes are not driven, such systems can be used for photon pair generation via a parametric conversion process [15–17]. As the effective nonlinearity decays quickly with the detuning from an atomic transition, the resulting photon pairs can be spectrally very narrow.

In this work, we investigate such a photon pair source based on four-wave mixing in a cold atomic ensemble. The resulting photon pairs are therefore directly compatible with ground state transitions of ^{87}Rb , and the pair preparation process does not suffer any reduction in brightness caused by additional filtering. This can be interesting for preparing photon states that are fragile with respect to linear losses. A basic description of the source

is presented in [18].

This source has already been used, with minor modifications, to obtain heralded single photons with an exponentially rising time envelope [19, 20]. We have also studied the amount of polarization entanglement in the generated photon pairs, and observed quantum beats between possible decay paths [21]. The same source has also been used in conjunction with a separate atomic system, a single ^{87}Rb atom trapped in a far off resonant focused beam to study their compatibility [22] and the dynamics of the absorption of single photons by an atom [23]. There, we explored a limited range of experimental parameters, optimized to observe the physical properties of the biphoton state of interest. In this article we present a systematic characterization of the source as function of the accessible experimental parameters. We believe that our scheme is a useful tool for the studies of the interaction of single photons with single and ensembles of atoms. In order to characterize the source, we focus our attention on generation rate, heralding efficiency, and the compromise between rates and bandwidth.

We start with a brief review of the photon pair generation process, followed by a presentation of the experimental setup, highlighting some of its relevant and differentiating features, and a description of the measurement technique. The rest of the paper covers systematic variations of the source parameters, and their impact on the rates and bandwidth of the emitted photon pairs.

II. FOUR WAVE MIXING IN COLD ^{87}Rb BASED ON CASCADE DECAY

The photon pair source in this work is based on the $\chi^{(3)}$ non-linear susceptibility of ^{87}Rb . A similar scheme was initially demonstrated with a different choice of transitions and, consequently, wavelengths [24]. The relevant electronic structure is shown in Fig. 1(a). Two pump beams of wavelength 780 nm (pump 1) and 776 nm (pump 2) excite the atoms from $5S_{1/2}, F=2$ to $5D_{3/2}, F=$

*christian.kurtsiefer@gmail.com

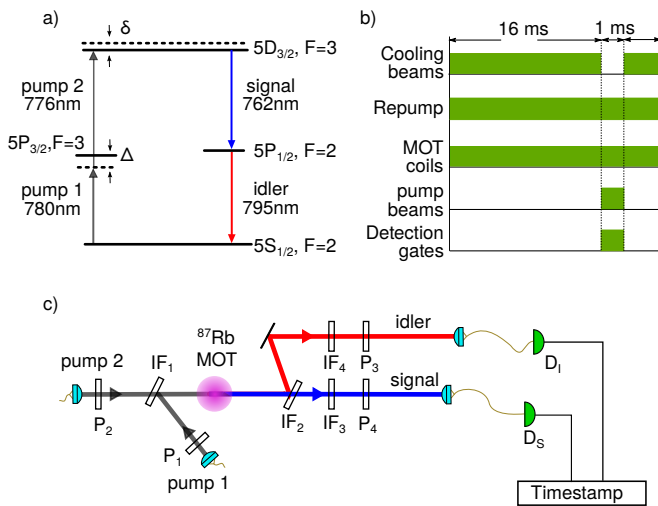


FIG. 1: (a) Cascade level scheme used for parametric conversion in atoms. (b) Timing sequence of the experiment. (c) Schematic of the experimental set up, with P1, P2, P3, and P4: Polarization filters, IF₁, IF₂, IF₃, and IF₄: interference filters, D₁, D₂: avalanche photodetectors.

3 via a two-photon transition. The 780 nm pump is red detuned by Δ from the intermediate level $5P_{3/2}, F=3$ to reduce the rate of incoherent scattering, with Δ between 30 and 60 MHz. The two-photon detuning δ is one of the parameters we study in this work.

The subsequent decay from the excited level $5D_{3/2}, F=3$ to the ground state $5S_{1/2}, F=2$ via $5P_{1/2}, F=2$ generates a pair of photons with wavelengths centered around 795 nm (signal) and 762 nm (idler). We reject light originating from other scattering processes using narrowband interference filters. The geometry of the pump and collection modes is chosen to satisfy the phase matching condition. Energy conservation ensures time correlation of the generated photons, while the time ordering imposed by the cascade decay results in a strongly asymmetrical time envelope of the biphoton. This coherent process is accompanied by incoherent scattering. Both processes generate light at the same wavelengths, making it impossible to distinguish them by spectral filtering. Similar to simple two-level systems [25, 26], coherent and incoherent scattering have different dependencies on a number of experimental parameters.

To understand the difference in behavior, we consider a long-established model of a strongly driven three-level atom [27, 28]. This simple model correctly describes some of the features of our photon pair source. In this model, the atomic state is described by the 3×3 density matrix ρ , where state 1 corresponds to the ground state, state 3 to the most excited state, and state 2 to the intermediate state in the cascade decay. The total scattering rate, that includes both coherent and incoherent events, is proportional to the population in state 3,

$$r_{\text{tot}} \propto \langle \rho_{33} \rangle, \quad (1)$$

while the signal we are interested in is proportional to the coherence between states 1 and 3,

$$r_{\text{coh}} \propto |\langle \rho_{31} \rangle|^2. \quad (2)$$

Following [27], we derive an analytical steady state solution of the master equation as function of the pump intensities (through the corresponding Rabi frequencies Ω_1 and Ω_2) and detunings (Δ and δ) [38].

In order to compare Eq. (1) and Eq. (2) to our experimental results, we need to take into account the linewidths of the pump lasers. A rigorous approach would require the inclusion of the laser linewidth in the master equation [29]. For large Rabi frequencies, as in our case, the spectral broadening associated with the laser power dominates. We can therefore approximate the combination of the two pump lasers Lorentzian profiles of width ≈ 1 MHz into a single noise spectrum with Gaussian profile $G(\delta)$ of width ≈ 2 MHz. We obtain a fitting function for our results by convolving Eq. (1) and (2) with the combined linewidth of the pump lasers,

$$r_{\text{single}} \propto r_{\text{tot}}(\Omega_1, \Omega_2, \Delta, \delta) * G(\delta), \quad (3)$$

and

$$r_{\text{pairs}} \propto r_{\text{coh}}(\Omega_1, \Omega_2, \Delta, \delta) * G(\delta). \quad (4)$$

The heralding efficiency for photons (in a scenario where one photon is used as a herald for the presence of the other) is the ratio of these rates:

$$\eta = \frac{r_{\text{pairs}}}{r_{\text{single}}} = \frac{r_{\text{coh}}(\Omega_1, \Omega_2, \Delta, \delta) * G(\delta)}{r_{\text{tot}}(\Omega_1, \Omega_2, \Delta, \delta) * G(\delta)}. \quad (5)$$

This model does not take into account the Zeeman manifold of the energy levels, nor the collective interaction within the atomic ensemble. We already presented a model and experimental evidence of the effects of polarization choice for pumps and collection modes previously [21]. In the rest of this article, the polarization of the pump beams and collection modes is chosen to maximize the effective nonlinearity and, consequently, maximize the generation rates. To understand the effect of collective interaction in a cascaded decay process we compare our results with the model proposed in [30] in section V.

III. EXPERIMENTAL SETUP

The experimental setup is shown in Fig. 1(c). The nonlinear medium is an ensemble of ^{87}Rb atoms in a vacuum chamber (pressure 1×10^{-9} mbar), trapped and cooled with a Magneto-Optical trap (MOT) formed by laser beams red detuned by 24 MHz from the cycling transition $5S_{1/2}, F=2 \rightarrow 5P_{3/2}, F=3$, with a diameter of 15 mm and an optical power of 45 mW per beam. An additional laser tuned to the $5S_{1/2}, F=1 \rightarrow 5P_{3/2}, F=2$ transition optically pumps the atoms back into the $5S_{1/2}, F=2$ level.

The low temperature of the ensemble ensures a negligible Doppler broadening of the atomic transition line, resulting in a reduction of the bandwidth of the generated photons by an order of magnitude compared to the hot vapor sources [31, 32].

In its initial implementation [18], the source was non-collinear, i.e., pump and collection modes do not lie on the same axis. This approach was chosen to minimize the collection of any pump light into the parametric fluorescence modes. In subsequent experiments, including this work, we instead chose a collinear configuration. This geometry simplifies the alignment and allows for a more efficient coupling of the generated photons into single mode fibers. We combine the pump beams (780 nm and 776 nm) using a narrowband interference filter (IF₁) as a dichroic mirror. Similarly, we separate the signal (762 nm) and idler (795 nm) modes using another interference filter (IF₂). Leaking of pump light into the collection modes is reduced by an additional interference filter in each collection mode (IF₃, IF₄). All interference filters used in the setup have a full width half maximum bandwidth of 3 nm and a peak transmission 96% at 780 nm. We tune their transmission frequencies by adjusting the angles of incidence. Polarizers P₁ and P₂ fix the polarization of the fluorescence before collecting it into single mode fibers with aspheric lenses. Single photons are detected using avalanche photo diodes (APD) with quantum efficiency of $\approx 50\%$.

Fig. 1(b) shows the timing sequence used in the experiment: 16 ms of cooling of the atomic vapors, followed by a 1 ms time window, during which the cooling beams are off and pump 1 and pump 2 shine on the cloud. We use external-cavity laser diodes (ECDL) with bandwidths in the order of 1 MHz to generate the pumps, and control their power and detuning using acousto-optic modulators (AOM).

IV. DETECTION OF PHOTON PAIRS

We characterize the properties of the source from the statistics and correlation of detection times for events in the signal and idler modes. All detection events are timestamped with a resolution of 125 ps. Fig. 2 shows a typical coincidence histogram $G^{(2)}$, i.e., the coincidence counts as a function of the delay between detection times Δt . The correlation function shows an asymmetric shape: a fast rise followed by a long exponential decay. The rise time is limited by the jitter time of the APDs (typical value ≈ 800 ps), while the decay is a function of the coherence time. In a previous work [18] we showed that the bandwidth is inversely proportional to the decay time constant τ . We measure τ by fitting the histogram $G^{(2)}$ with the function

$$G_{\text{fit}}^{(2)}(\Delta t) = G_{\text{acc}} + G_0 e^{-\Delta t/\tau} \Theta(\Delta t), \quad (6)$$

where G_{acc} is the rate of accidental coincidences, Θ is the Heaviside step function, and G_0 an amplitude. The rate

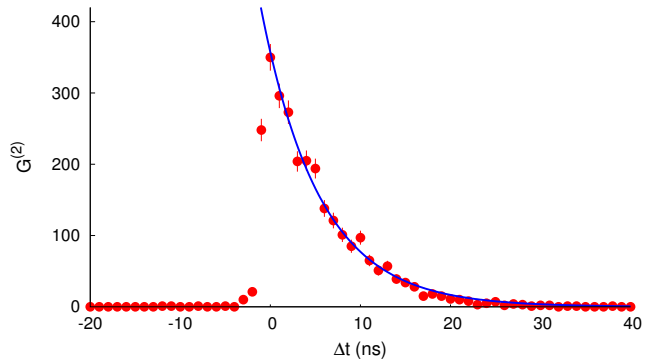


FIG. 2: Histogram of coincidence events $G^{(2)}(\Delta t)$ as a function of the time difference between the detection of signal and idler photons for a total integration time of 42 s. Pump powers: $P_{780} = 450 \mu\text{W}$ and $P_{776} = 3 \text{mW}$, detunings $\Delta = -60 \text{MHz}$ and $\delta = 12 \text{MHz}$. The solid line is a fit to the model described by Eq. 6, giving a value of $\tau = 6.52 \pm 0.04 \text{ns}$.

of accidental coincidences G_{acc} is fixed by considering the average of $G^{(2)}$ for times Δt much larger than the coherence time, leaving as free parameters only G_0 and τ .

To characterize the source, we consider the rate of single event detection in the signal (r_s) and idler (r_i) modes, together with the rate of coincidence detection (r_p) as the signature of photon pairs. All reported rates are instantaneous rates in the parametric conversion part of the cooling/photon generation cycle.

The total pair detection rate r_p of the source is obtained by integrating $G^{(2)}(\Delta t)$ over a coincidence time window $0 < \Delta t < \Delta t_c$. We choose $\Delta t_c = 30 \text{ns}$ to ensure the collection of a large fraction of events also for the largest coherence times τ observed.

Another parameter we extract from the measured $G^{(2)}(\Delta t)$ is heralding efficiency. Due to the intrinsic asymmetry of the process we define a two heralding efficiencies from the same measurement, one for the signal,

$$\eta_S = r_p / (r_S - d_S), \quad (7)$$

and one for the idler,

$$\eta_I = r_p / (r_I - d_I), \quad (8)$$

where $d_S = 508 \text{s}^{-1}$ and $d_I = 165 \text{s}^{-1}$ are the dark count rates on the signal and idler detectors.

V. EFFECT OF THE NUMBER OF ATOMS

One of the parameters of interest is the number of atoms N participating in the four-wave mixing process. We control it by varying the optical power of the repump light during the cooling phase, thus changing the atomic density without altering the geometry of the optical trap.

We estimate N by measuring the optical density (OD) of the atomic ensemble for light resonant with

the $5S_{1/2}, F = 2 \rightarrow 5P_{3/2}, F = 3$ transition. To obtain a reliable measure of the OD, we turn off pump 2 and set pump 1 to $10 \mu\text{W}$, more than 40 times lower than the saturation intensity of the transition of interest. We record the transmission of pump 1 through the vacuum cell for a range of values of Δ wide enough to capture the entire absorption feature, and normalize it to the transmission observed without the atomic cloud. We fit the measurement results with the expected transmission spectrum

$$T(\Delta) = \exp\left(-\text{OD} \frac{\gamma^2}{\Delta^2 + \gamma^2}\right), \quad (9)$$

with $\gamma = 6.067 \text{ MHz}$ and OD as the only free parameter. From the size of the probe beam $w_0 \approx 450 \mu\text{m}$, we estimate N . We observed a minimum of $N \approx 1.5 \times 10^7$, corresponding to an $\text{OD} \approx 7$, and a maximum of $N \approx 6.3 \times 10^7$, $\text{OD} \approx 29$. We expect the effective number of atoms participating in the FWM process to decrease during the measurement due to the heating caused by the intense pumps.

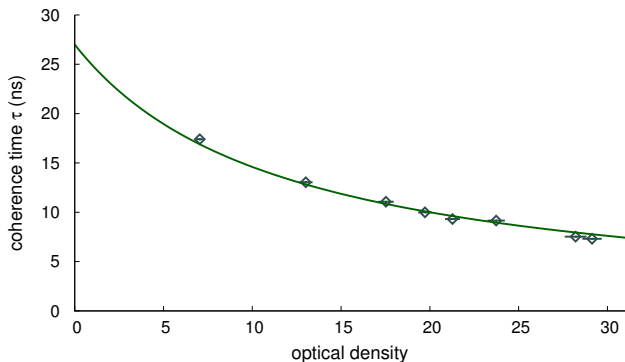


FIG. 3: Coherence time of the photon pair as a function of the optical density (OD) of the atomic cloud. The solid line is obtained by fitting Eq. 10, obtaining $\mu = 0.0827 \pm 0.002$. Other parameters: $P_{776} = 15 \text{ mW}$, $P_{780} = 300 \mu\text{W}$, $\Delta = -60 \text{ MHz}$, $\delta = 12 \text{ MHz}$.

Single detection rates for the signal (r_s) and idler (r_i) modes increase linearly with the number of atoms involved in the process, as expected for incoherent processes (see Fig. 4). The increase of pair rate r_p with N , however, appears to be faster than linear.

Further, the decay or coherence time τ decreases in our experiments as OD increases (see Fig. 3). The measured coherence time is always shorter than the natural lifetime $\tau_0 = 27 \text{ ns}$ of the intermediate state expected for the spontaneous decay in free space of this transition to the ground state of ^{87}Rb . This is a signature of collective effects in the cold atom cloud [18, 33]. The solid line is a fit to the theoretical model proposed in [30]:

$$\tau = \frac{\tau_0}{1 + \mu \text{OD}}, \quad (10)$$

where the free parameter μ is a geometrical constant depending on the shape of the atomic ensemble.

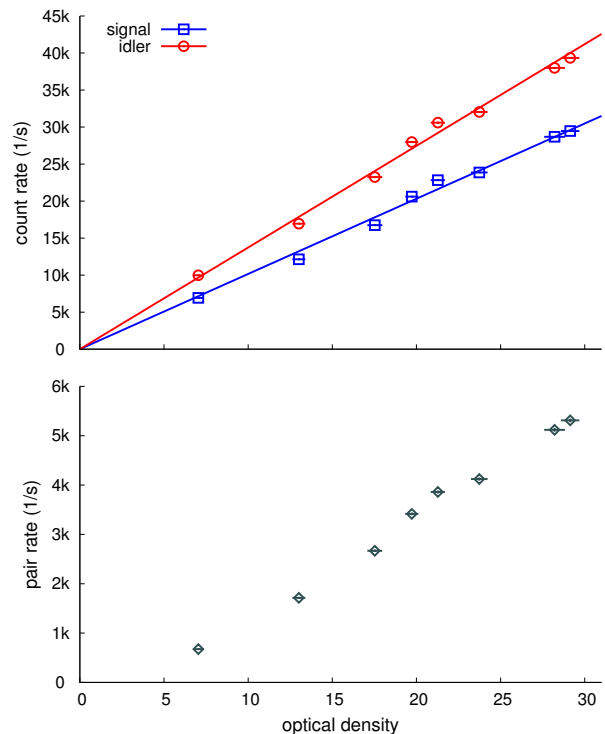


FIG. 4: Rate of single counts in the signal and idler modes (top), and rate of coincidence counts (bottom) as a function of the optical density (OD) of the atomic cloud. The solid lines are fits for $r_{s,i} = a_{s,i} \text{OD}$, with $a_{s,i}$ the only free parameter. Other parameters: $P_{776} = 15 \text{ mW}$, $P_{780} = 300 \mu\text{W}$, $\Delta = -60 \text{ MHz}$, $\delta = 12 \text{ MHz}$.

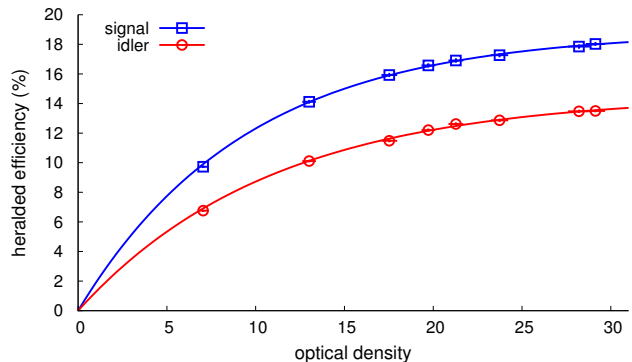


FIG. 5: Heralding efficiency for signal and idler modes as a function of the optical density. The solid lines are fits of Eq. 11 with $\eta_{0s} = 0.190 \pm 0.001$ and $\text{OD}_{0s} = 9.7 \pm 0.1$, and $\eta_{0i} = 0.150 \pm 0.001$ and $\text{OD}_{0i} = 11.3 \pm 0.2$. Other parameters: $P_{776} = 15 \text{ mW}$, $P_{780} = 300 \mu\text{W}$, $\Delta = -60 \text{ MHz}$, $\delta = 12 \text{ MHz}$.

We do not have a complete explanation for the non-linear increase of the pair rate with the optical density, but some insight can be gained from the heralding efficiencies shown in Fig. 5. Both heralding efficiencies η_s and η_i exhibit a saturation behavior that is described by

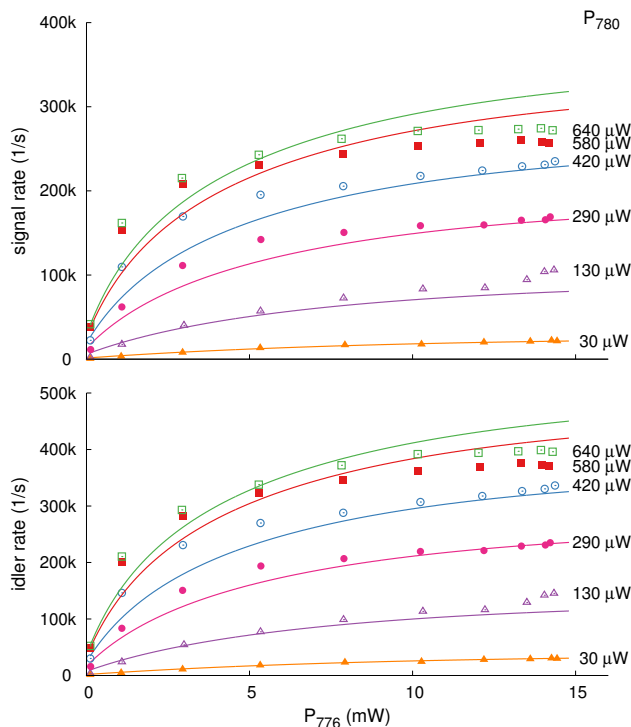


FIG. 6: Single rates for the signal (top) and idler (bottom) as a function of pump power at 776 nm (P_{776}) for different pump powers at 780 nm. The vertical error bar on each point is smaller than the size of the data points. Other parameters: $OD = 29$, $\Delta = -60$ MHz, $\delta = 3$ MHz. The solid lines are numerical fits with Eq. 3.

the relation

$$\eta_j = \eta_{0j} \left[1 - \exp\left(-\frac{OD}{OD_{0j}}\right) \right] \quad \text{with } j = s, i, \quad (11)$$

where η_{0j} and OD_{0j} are free parameters. This heuristic expression suggests that (a) a higher optical density of the atomic cloud leads to an increase of the pair rate at the expense of a larger photon bandwidth, and (b) for large enough OD there is no improvement of heralding efficiency. Such considerations are discussed in section IX.

VI. RATES AND HERALDING EFFICIENCIES

Brightness, a common parameter to characterize a photon pair source, is defined as the experimentally accessible rate of photon pairs emitted into the desired modes per mW of pump power. In our source, saturation effects of the atomic transitions involved give rise to a non-linear correlation between pump power and rates. In Fig. 6 and 7, the instantaneous single rates, r_s and r_i , and pair rates r_p as a function of power in both pump transitions are shown.

For a fixed two-photon detuning δ , all rates exhibit a saturation behavior. This suggests that an increase

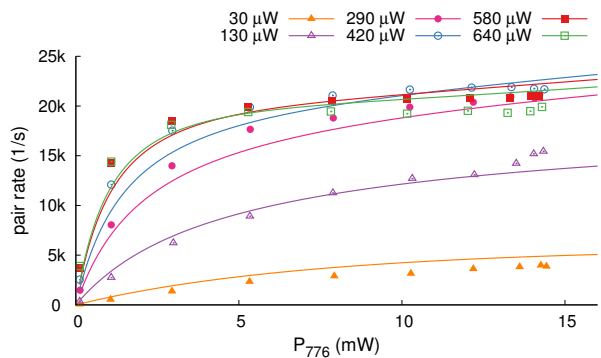


FIG. 7: Pair rates as function of pump power at 776 nm (P_{776}) for different pump powers at 780 nm. The vertical error bar on each point is smaller than the size of the data points. The solid lines are calculated from the theory. Other parameters: $OD = 29$, $\Delta = -60$ MHz, $\delta = 3$ MHz. The solid lines are numerical fits with Eq. 4.

of the pump powers will increase the observed pair rate only to some extent, and an increased number of atoms of the ensemble might be a better option. However, as discussed in the previous section, this comes at the expense of a larger bandwidth. We also note that, while the model introduced in section II qualitatively explains the saturation behavior with the pump powers, it does not capture well the experimental observation for high powers. This is probably due to the optical pumping caused by the intense pump beams, which is not part of the relatively simple model.

The dependency of heralding efficiencies on both pump powers is shown in Fig. 8, both for our experimental observations and the model predictions.

The intuition of a higher heralding efficiency at low pump powers due to a smaller contribution from incoherent processes is both found in the experiment and predicted by the model, but the model does not match the observations at low powers very well. A possible explanation is in one of the assumptions of our model. For low pump powers, the broadening due to Rabi frequencies of the pumps is comparable with the pump lasers linewidths, requiring then a different approach than convolution with a combined noise spectrum. However, our simple model ignores all geometrical aspects in the process, and therefore does not capture any spatial variation of the atomic density profile of the cloud, the intensity profile of the pump beams, or their respective overlap.

Despite the limitations of the model, the observed power dependency of pair rates and heralding efficiency shown in Fig. 7 and 8 suggest a strategy for optimizing the source brightness: a low power P_{780} on the transition depopulating the ground state should ensure a high heralding efficiency, while a high power P_{776} on the transition populating the state 3 should increase the brightness. An obvious experimental limitation to this strategy for Rubidium is the available P_{776} .

Apart from the optical power in the pump beams, other

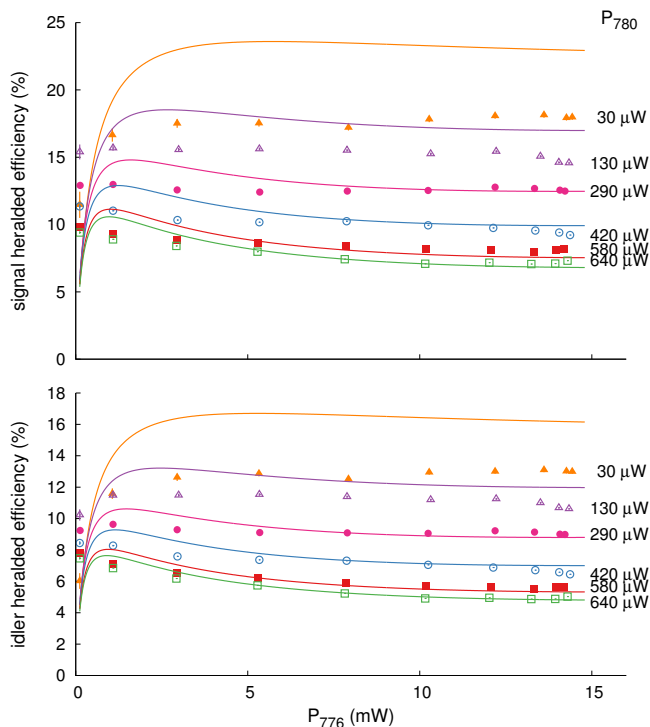


FIG. 8: heralding efficiency as function of P_{776} for the signal (top) and idler (bottom) for different P_{780} . The vertical error bar on each point is smaller than the size of the data points. Other parameters: $OD=29$, $\Delta = -60$ MHz, $\delta = 3$ MHz. The solid lines are a numerical fit with Eq. 5.

easily available experimental parameters in the four wave mixing process are the pump detunings. Both single and pair rates have a strong dependence on the two-photon detuning δ from the ground state in the upper excited state, and have a maximum at $\delta \approx 0$, as expected for a scattering process (see Fig. 9). The two-step nature of the excitation process leads to asymmetries in the peaks, which is also predicted by the simple model of Eq. (3) and (4). To allow for a fair comparison between the model prediction and the experimental data, we have to take into account the linewidth of the pump lasers (≈ 1 MHz each). We therefore convolve the theoretical predictions in Equations 3 and 4 with a Gaussian distribution modeling our laser noise. The resulting spectral profiles in the two-photon detuning of pair and single rates then match very well the behavior observed in our experiment.

Contrary to the single and pair rates, both heralding efficiencies show an asymmetric dip around $\delta \approx 0$ (see Fig. 10) in our experiment, which is well captured by the model via Eq. 5.

This dip can be understood by taking into account that the observed single rate is the combination of FWM, a coherent process, and incoherent scattering, with the latter growing faster as δ approaches 0. When choosing the operation parameter of a photon pair source for subsequent

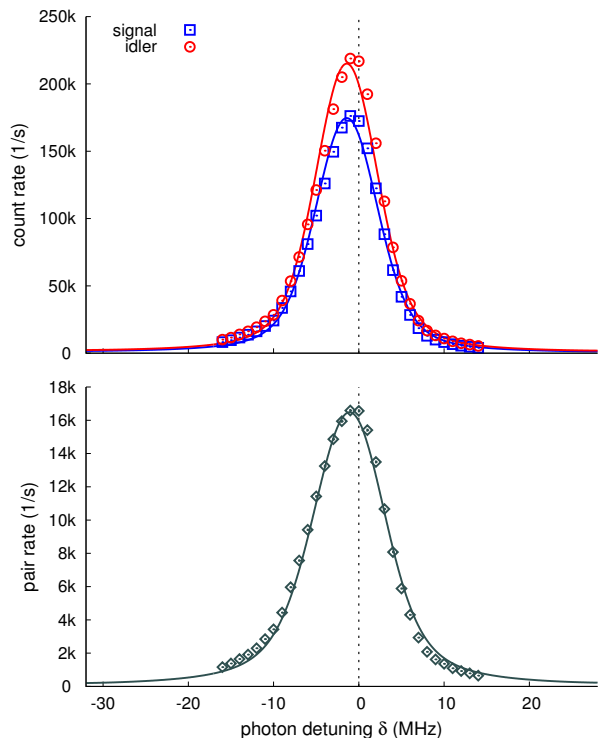


FIG. 9: (Top) Single count rates as a function of the detuning from the two photon resonance δ . The solid lines are numerical fits of Eq. 3. (Bottom) Pair rate (r_p) as a function of δ . The solid line is a numerical fit of Eq. 4. Other parameters: $P_{776} = 15$ mW, $P_{780} = 450 \mu\text{W}$, $\Delta = -60$ MHz, $OD=29$. The dotted line indicates $\delta = 0$.

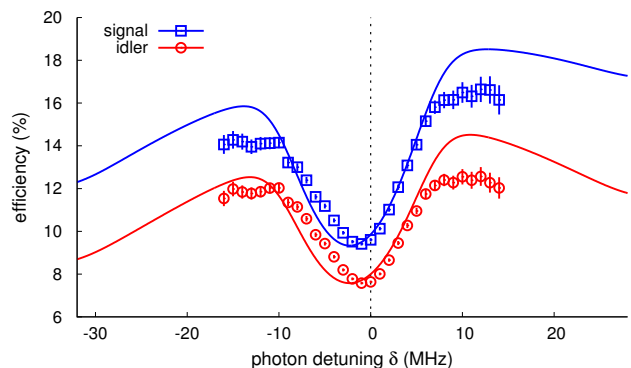


FIG. 10: Efficiency of the source as a function of the detuning from the two photon resonance δ . Other parameters: $P_{776} = 15$ mW, $P_{780} = 450 \mu\text{W}$, $\Delta = -60$ MHz, $OD=29$. The solid lines are fits with Eq. 5, the dotted line indicates $\delta = 0$.

use, the two-photon detuning can therefore be optimized for a compromise between pair rate and heralding efficiency.

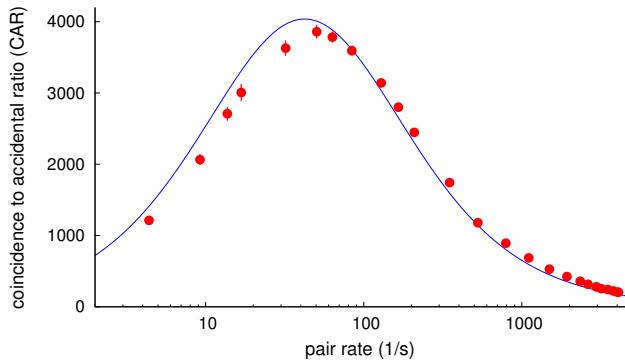


FIG. 11: The coincidence to accidental ratio (CAR) as a function of pair rates r_p . The solid line is obtained from Eq. (13) with $\eta_S = 17.3\%$, $\eta_I = 12.4\%$, $d_S = 165 \text{ s}^{-1}$, $d_I = 508 \text{ s}^{-1}$, $\Delta t = 30 \text{ ns}$.

VII. COINCIDENCE TO ACCIDENTAL RATIO (CAR)

Another relevant parameter for characterizing the usefulness of a source of photon pairs is the coincidence to accidental ratio (CAR) [34, 35],

$$\text{CAR} = \frac{R_p}{r_a} = \frac{r_I r_S \Delta t + r_p}{r_I r_S \Delta t}, \quad (12)$$

where the accidental rate r_a captures noise photons that degrade the correlation characteristics of the photon pair source. The connection between the CAR and pair rate r_p is shown in Fig. 11. In this parametric plot, we vary the pump power P_{776} . Over a wide range of pair rates, the CAR increases when P_{776} is reduced because $r_a \propto r_p^2$. For the experimental parameters shown in this measurement, the CAR peaks at ≈ 3800 , at a relatively low pair rate of $r_p = 50 \text{ s}^{-1}$. With a further reduction in pump power (and therefore in r_p), the CAR drops to 1, as background noise and detector's dark counts (r_a) dominate in Eq. 12.

To model the experimentally observed CAR, we modify the expression in Eq. 12 by separating the single rates for signal and idler into a contribution from pairs, corrected by the respective heralding efficiencies, and dark/background contributions for signal and idler. Signal and idler heralding efficiencies vary very little over a wide range of pump powers P_{776} , so we fix them to a single value. The resulting expression for the CAR,

$$\text{CAR} = \frac{\left(\frac{r_p}{\eta_S} + d_S\right) \left(\frac{r_p}{\eta_I} + d_I\right) \Delta t + r_p}{\left(\frac{r_p}{\eta_S} + d_S\right) \left(\frac{r_p}{\eta_I} + d_I\right) \Delta t}, \quad (13)$$

reproduces very well the observed behavior in the experiment, suggesting that the relation between CAR and pair rates is fairly well understood.

VIII. COHERENCE TIME OF THE GENERATED PAIRS

An important property of photon pair sources based on nonlinearities is the small bandwidth of the emerging photons corresponding to a long coherence time. The dependency of the coherence time, measured by fitting photon pair timing histograms to Eq. 6, on pump power and two-photon detuning is shown in Fig. 12 and 13. The coherence time increases with both pump powers, and also shows a maximum with respect to the two-photon detuning slightly below the two-photon resonance, similar to the pair rates.

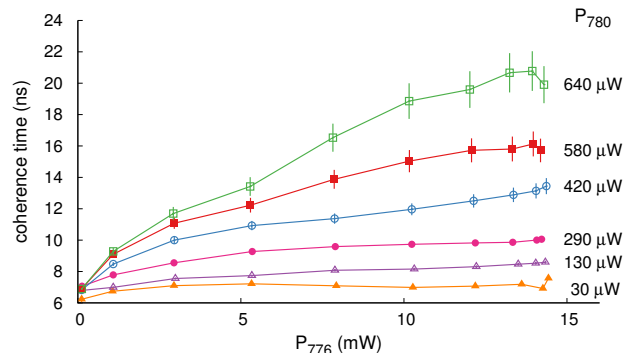


FIG. 12: Coherence time as function of pump powers. Other parameters: $\text{OD} = 29$, $\Delta = -60 \text{ MHz}$, $\delta = 3 \text{ MHz}$.

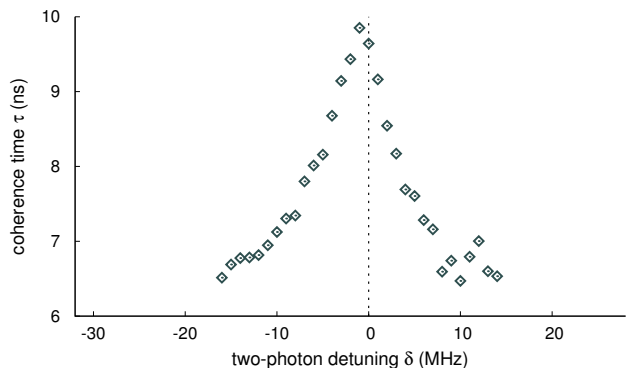


FIG. 13: Coherence time as function of detuning. Other parameters: $P_{776} = 15 \text{ mW}$, $P_{780} = 450 \mu\text{W}$, $\Delta = -60 \text{ MHz}$, $\text{OD} = 29$. The dotted line indicates $\delta = 0$.

The simple 3-level model in section II does not address the coherence time of the emerging photons. Even a more complex model that includes the collective effects associated with the number of atoms [30] predicts only a dependency of the coherence time on the number of atoms involved in the four-wave mixing process (superradiance), but not on the pump power and two-photon detuning. A possible reason for the observed dependency is a decay from the excited state $5P_{1/2}$, $F = 3$ to $5S_{1/2}$, $F = 1$, a ground state that does not participate in

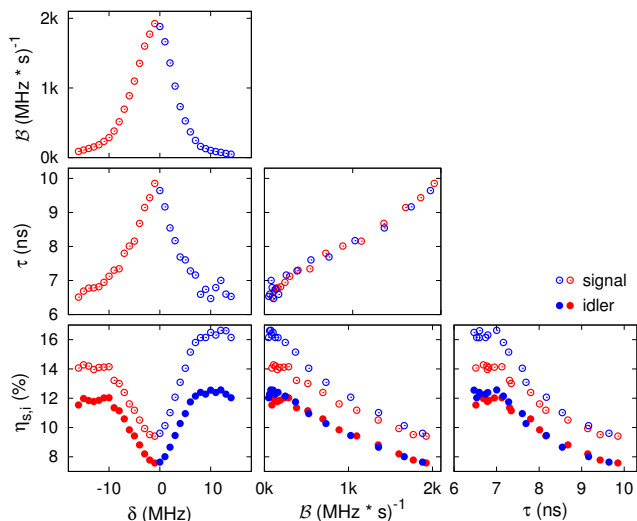


FIG. 14: Summary of the effect of two-photon detuning δ on heralding efficiencies $\eta_{s,i}$, coherence time τ , and spectral brightness \mathcal{B} . Other parameters: $P_{776} = 15$ mW, $P_{780} = 450$ μ W, $\Delta = -60$ MHz, OD=29.

the coherent four wave mixing we are interested in, effectively depleting the number of atoms interacting with the pump beams. This depletion increases with pump intensities, and decreases with detuning, and is not completely neutralized by the repump beam, resulting in a change of the number of atoms in the participating ground state, which would then affect the coherence time according to the more complex conversion model [30].

To arrive at long coherence times, one therefore would need to optimize the repumping process during the parametric conversion cycle in our experiment to maintain the atomic population in the ground state.

IX. GUIDELINES FOR CHOICE OF PARAMETERS

Following our characterization of this photon pair source, it is useful to introduce some guidelines for the choice of operational parameters. We summarize the effects of the different experimental knobs in Fig. 14, 15, and 16. We included the heralding efficiency, coherence times, and spectral brightness $\mathcal{B} = 2\pi \cdot \tau \cdot r_p$. Some trends are common: heralding efficiencies and coherence time appear to be inversely correlated, independently of the parameters we are varying. In experiments where the generated photon pairs interact with atomic systems it is often important to maximize the spectral brightness. In this case, it is necessary to maximize the optical density, set the two-photon detuning a few MHz red off resonance, and maximize both pump powers. If the target is to maximize the heralding efficiency, it is convenient to increase the two-photon detuning, and reduce power P_{780} until a suitable compromise between heralding efficiency and

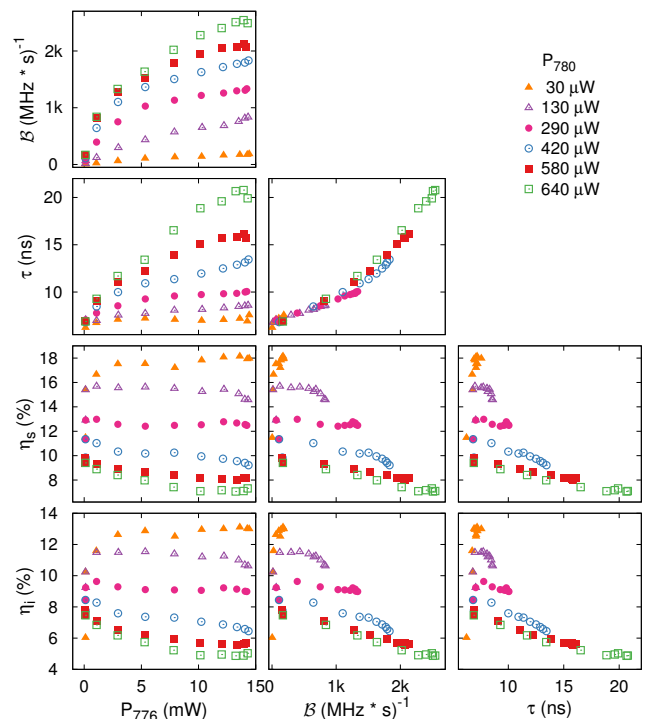


FIG. 15: Summary of the effect of pump powers P_1 and P_2 on heralding efficiencies $\eta_{s,i}$, coherence time τ , and spectral brightness \mathcal{B} . Other parameters: OD=29, $\Delta = -60$ MHz, $\delta = 3$ MHz.

brightness is reached.

X. CONCLUSION

We presented an experimental study of the effect of two-photon detuning, pump intensity, and number of atoms on the generation rates and bandwidth of photon pairs from four-wave mixing in a cold ensemble of rubidium atoms. The study is useful to understand how to set the different parameters to better exploit the source characteristics, in particular when combined with other, generally very demanding, atomic systems [22, 23].

The effect of pump powers and two-photon detuning on pair rates and efficiencies are compatible with the theoretical model presented by Whitley and Stroud [27]. An increase in pump power corresponds to an increase of pair and singles rates until a saturation level, with heralding efficiency determined mostly by the ground-state resonant pump. We can also explain the connection between the coincidence to accidentals ratio (CAR) and the generated pair rates. All rates increase with a reduction of the two-photon detuning at the expenses of heralding efficiency. This is well captured by the model, and can be intuitively explained as the result of competition between coherent and incoherent scattering processes excited by the same optical pumps.

One of the attractive aspects of cold-atoms based pho-

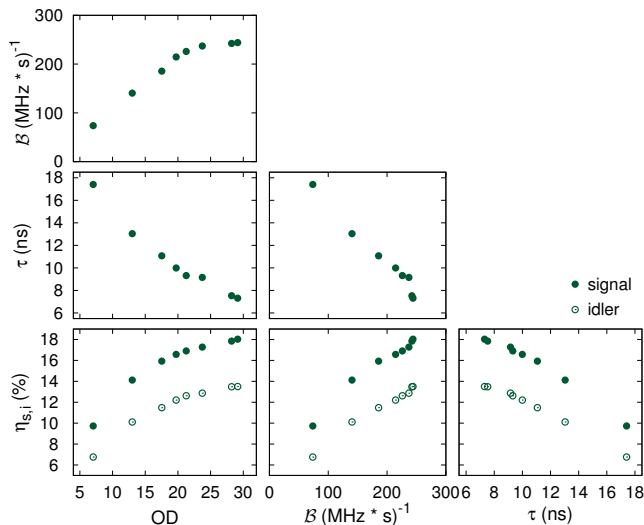


FIG. 16: Summary of the effect of optical density OD on heralding efficiencies $\eta_{s,i}$, coherence time τ , and spectral brightness B . Other parameters: $P_{776} = 15$ mW, $P_{780} = 300$ μ W, $\Delta = -60$ MHz, $\delta = 12$ MHz.

ton pairs sources is their frequency characteristics: the generated pairs are usually resonant or close to resonant with their bandwidth of the same order of magnitude as atomic transitions. In our source the central wave-

lengths are fixed, the bandwidth instead is a function of the experimental parameters, in particular of the number of atoms. The dipole-dipole interaction between atoms gives rise to superradiance [36], as evidenced by the reduction of coherence time as the number of atoms increases [30]. But the total number of atoms is also a function of duration, intensity, and detuning of the pump beams because of optical pumping. The dynamics of the combined effect of collective interaction between atoms and optical pumping increases the complexity of the phenomenon, and we currently do not have a model that fully explain our result. Nonetheless, the experimental measurements are a useful guide to choose the number of atoms, together with the other parameters, that optimizes the specific properties desired from the source: rate, heralding efficiency, or bandwidth.

XI. ACKNOWLEDGMENTS

We like to thank Mathias A. Seidler, Matthias Steiner, and Chin Yue Sum for useful discussions about the theoretical modeling of the source. This work was supported by the Ministry of Education in Singapore and the National Research Foundation, Prime Minister's office (partly under grant no NRF-CRP12-2013-03).

-
- [1] J. F. Clauser and A. Shimony, Rept.Prog.Phys. **41**, 1881 (1978).
- [2] A. Aspect, P. Grangier, and G. Roger, Phys. Rev. Lett. **47**, 460 (1981).
- [3] A. K. Ekert, Phys. Rev. Lett. **67**, 661 (1991).
- [4] D. Bouwmeester, J.-W. Pan, K. Mattle, M. Daniell, A. Zeilinger, and H. Weinfurter, Nature **390**, 575 (1997).
- [5] D. Boschi, S. Branca, F. De Martini, L. Hardy, and S. Popescu, Phys. Rev. Lett. **301**, 1121 (1998).
- [6] D. C. Burnham and D. L. Weinberg, Phys. Rev. Lett. **25**, 84 (1970).
- [7] P. G. Kwiat, K. Mattle, H. Weinfurter, A. Zeilinger, A. V. Sergienko, and Y. Shih, Phys. Rev. Lett. **75**, 4337 (1995).
- [8] C. Kurtsiefer, M. Oberparleiter, and H. Weinfurter, Phys. Rev. A **64**, 023802 (2001).
- [9] C. E. Kuklewicz, F. N. C. Wong, and J. H. Shapiro, Phys. Rev. Lett. **97**, 223601 (2006).
- [10] F. Wolfgramm, X. Xing, A. Cerè, A. Predojević, A. M. Steinberg, and M. W. Mitchell, Opt. Express **16**, 18145 (2008).
- [11] J. Fekete, D. Rielander, M. Cristiani, and H. de Riedmatten, Phys. Rev. Lett. **110**, 220502 (2013).
- [12] J. S. Neergaard-Nielsen, B. M. Nielsen, B. M. Nielsen, H. Takahashi, A. I. Vistnes, and E. S. Polzik, Opt. Express **15**, 7940 (2007).
- [13] A. Haase, N. Piro, J. Eschner, and M. W. Mitchell, Opt. Lett. **34**, 55 (2009).
- [14] G. Schunk, U. Vogl, F. Sedlmeir, D. V. Strekalov, A. Ottterpohl, V. Averchenko, H. G. L. Schwefel, G. Leuchs, and C. Marquardt, Journal of Modern Optics, **1** (2016).
- [15] D. A. Braje, V. Balić, S. Goda, G.-Y. Yin, and S. E. Harris, Phys. Rev. Lett. **93**, 183601 (2004).
- [16] D. N. Matsukevich, M. Bhattacharya, S. Y. Lan, S. D. Jenkins, and A. Kuzmich, Phys. Rev. Lett. **95**, 040405 (2005).
- [17] J. F. Chen and S. Du, Front. Phys. **7**, 494 (2012).
- [18] B. Srivathsan, G. K. Gulati, B. Chng, G. Maslennikov, D. N. Matsukevich, and C. Kurtsiefer, Phys. Rev. Lett. **111**, 123602 (2013).
- [19] G. K. Gulati, B. Srivathsan, B. Chng, A. Cerè, D. Matsukevich, and C. Kurtsiefer, Phys. Rev. A **90**, 033819 (2014).
- [20] B. Srivathsan, G. K. Gulati, A. Cerè, B. Chng, and C. Kurtsiefer, Phys. Rev. Lett. **113**, 163601 (2014).
- [21] G. K. Gulati, B. Srivathsan, B. Chng, A. Cerè, and C. Kurtsiefer, New J. Phys. **17**, 093034 (2015).
- [22] V. Leong, S. Kosen, B. Srivathsan, G. K. Gulati, A. Cerè, and C. Kurtsiefer, Phys. Rev. A **91**, 063829 (2015).
- [23] V. Leong, M. A. Seidler, M. Steiner, A. Cerè, and C. Kurtsiefer, Nat Comms **7**, 13716 (2016).
- [24] T. Chanelière, D. N. Matsukevich, and S. D. Jenkins, Phys. Rev. Lett. **96**, 093604 (2006).
- [25] B. R. Mollow, Phys. Rev. **188**, 1969 (1969).
- [26] C. Cohen-Tannoudji, J. Dupont-Roc, and G. Grynberg, "Optical bloch equations," in *Advances in Cryptology - Proc. Eurocrypt'94* (Wiley-VCH Verlag GmbH, 1994) pp. 353–405.
- [27] R. M. Whitley and J. C R Stroud, Phys. Rev. A **14**, 1498

- (1976).
- [28] S. V. Lawande, R. R. Puri, and R. D'Souza, Phys. Rev. A **33**, 2504 (1986).
- [29] M. J. McDonnell, D. N. Stacey, and A. M. Steane, Phys. Rev. A **70**, S123 (2004).
- [30] H. H. Jen, J. Phys. B: At. Mol. Opt. Phys. **45**, 165504 (2012).
- [31] R. T. Willis, F. E. Becerra, L. A. Orozco, and S. L. Rolston, Phys. Rev. A **82**, 053842 (2010).
- [32] D.-S. Ding, Z.-Y. Zhou, B.-S. Shi, X.-B. Zou, and G.-C. Guo, Opt. Express **20**, 11433 (2012).
- [33] M. Gross and S. Haroche, Physics Reports **93**, 301 (1982).
- [34] H. Takesue and K. Shimizu, Opt. Commun. **283**, 276 (2010).
- [35] C. Xiong, G. D. Marshall, A. Peruzzo, M. Lobino, A. S. Clark, D. Y. Choi, S. J. Madden, C. M. Natarajan, M. G. Tanner, R. H. Hadfield, S. N. Dorenbos, T. Zijlstra, V. Zwiller, M. G. Thompson, J. G. Rarity, M. J. Steel, B. Luther-Davies, B. J. Eggleton, and J. L. O'Brien, Appl. Phys. Lett. **98**, 051101 (2011).
- [36] R. H. Dicke, Phys. Rev. **93**, 99 (1954).
- [37] A. V. Akimov, E. O. Tereshchenko, S. A. Snigirev, A. Y. Samokotin, A. V. Sokolov, and V. N. Sorokin, Quantum Electron. **40**, 139 (2010).
- [38] These analytical forms are long and cumbersome, we have included them in the appendix. Note that the solutions presented in [27] contain a mistake, as already pointed out by [37]

Appendix A: Explicit form of Eq. (1) and Eq. (2)

$$\langle \rho_{33} \rangle = \frac{\Omega_1^2 \Omega_2^2 (\Gamma_1 \Gamma_2 ((\delta - \Delta)^2 + (\Gamma_1 + \Gamma_2)^2) + \Gamma_1 \Omega_1^2 (\Gamma_1 + \Gamma_2) + \Omega_2^2 (\Gamma_1 + \Gamma_2)^2)}{K} \quad (\text{A1})$$

$$\begin{aligned} |\langle \rho_{31} \rangle|^2 = & \left| \frac{\Omega_1 \Omega_2}{K} \right|^2 \cdot \left| \delta^3 \Gamma_1 \Gamma_2 (\Delta - i\Gamma_1) - \delta^2 \Gamma_1 \Gamma_2 ((\Delta - i\Gamma_1)(2\Delta + i\Gamma_2) + \Omega_1^2 + \Omega_2^2) \right. \\ & + \delta \Gamma_1 (\Gamma_2 (\Delta - i\Gamma_1) (\Delta^2 + 2i\Delta\Gamma_2 + (\Gamma_1 + \Gamma_2)^2) + \Omega_2^2 (\Delta(\Gamma_1 + 3\Gamma_2) - i\Gamma_1(\Gamma_1 + \Gamma_2)) + 2i\Gamma_2 \Omega_1^2 (\Gamma_1 + \Gamma_2)) \\ & - i\Delta^3 \Gamma_1 \Gamma_2^2 - \Delta^2 \Gamma_1 \Gamma_2 (\Gamma_1 \Gamma_2 - \Omega_1^2 + \Omega_2^2) - i\Delta \Gamma_1 \Gamma_2 (\Gamma_1 + \Gamma_2) (\Gamma_2 (\Gamma_1 + \Gamma_2) + 2\Omega_1^2 + \Omega_2^2) \\ & \left. - (\Gamma_1 \Gamma_2 (\Gamma_1 + \Gamma_2) + \Gamma_1 \Omega_2^2 - \Gamma_2 \Omega_1^2) (\Gamma_1 (\Gamma_2 (\Gamma_1 + \Gamma_2) + \Omega_1^2) + \Omega_2^2 (\Gamma_1 + \Gamma_2)) \right|^2 \end{aligned} \quad (\text{A2})$$

with

$$\begin{aligned} K = & \delta^4 \Gamma_1 \Gamma_2 (\Delta^2 + \Gamma_1^2 + 2\Omega_1^2) - 2\delta^3 \Delta \Gamma_1 \Gamma_2 (\Delta^2 + \Gamma_1^2 + 2\Omega_1^2 + \Omega_2^2) \\ & + \delta^2 (\Omega_2^2 (\Delta^2 \Gamma_1 (\Gamma_1 + 5\Gamma_2) + \Gamma_1^2 (\Gamma_1^2 + \Gamma_1 \Gamma_2 + 2\Gamma_2^2)) + 2\Omega_1^2 (\Gamma_1 + \Gamma_2)^2) \\ & + \Gamma_1 \Gamma_2 (\Delta^2 + \Gamma_1^2 + 2\Omega_1^2) (\Delta^2 + \Gamma_1^2 + 2\Gamma_1 \Gamma_2 + 2\Gamma_2^2 - 2\Omega_1^2) + \Gamma_1 \Gamma_2 \Omega_2^4 \\ & + 2\delta \Delta (-\Gamma_2 \Omega_2^2 (\Gamma_1 (\Delta^2 + \Gamma_1^2 + 4\Gamma_1 \Gamma_2 + \Gamma_2^2) + \Gamma_2 \Omega_1^2) + \Gamma_1 \Gamma_2 (\Omega_1^2 - \Gamma_2^2) (\Delta^2 + \Gamma_1^2 + 2\Omega_1^2) - \Gamma_1 \Omega_2^4 (\Gamma_1 + 2\Gamma_2)) \\ & + \Delta^4 \Gamma_1 \Gamma_2^3 + \Delta^2 \Gamma_2 (\Gamma_1 (\Gamma_2^2 (2\Gamma_1^2 + 2\Gamma_1 \Gamma_2 + \Gamma_2^2) + 2\Gamma_2 \Omega_1^2 (\Gamma_1 + 2\Gamma_2) + \Omega_1^4) + \Gamma_2 \Omega_2^2 (\Gamma_1 (3\Gamma_1 + \Gamma_2) + \Omega_1^2) + \Gamma_1 \Omega_2^4) \\ & + (\Gamma_2 (\Gamma_1 + \Gamma_2) + \Omega_1^2 + \Omega_2^2) (\Gamma_1^2 \Gamma_2 + \Gamma_1 \Omega_2^2 + 2\Gamma_2 \Omega_1^2) (\Gamma_1 (\Gamma_2 (\Gamma_1 + \Gamma_2) + \Omega_1^2) + \Omega_2^2 (\Gamma_1 + \Gamma_2)) , \end{aligned} \quad (\text{A3})$$

where Γ_1 and Γ_2 are the linewidths of the transitions addressed by pump 1 and 2, respectively.